ADVANCED FUNCTIONAL MATERIALS
www.afm-journal.de

Twisting Between Topological Phases in 1D Conjugated Polymers via a Multiradical Transition State

Isaac Alcón, Luis Manuel Canonico, Nick Papior, Jose-Hugo Garcia, Aron W. Cummings, Jean-Christophe Tremblay, Miguel Pruneda,* Mads Brandbyge, Beate Paulus, and Stephan Roche*

In recent years, it has become possible via on-surface bottom-up synthesis to engineer the topological character of carbon nanostructures. Graphene nanoribbons and 1D conjugated polymers (1DCPs) have thus tailored so as to host either topologically trivial or non-trivial phases. Molecular design is the primary means to set the topological class of these nanomaterials. However, external control over topology is also demonstrated via electric fields or top-down hydrogenation. Inspired by the connection between topology and π-conjugation, here it is demonstrated via first-principles calculations that aryl ring twist angles also serve as topological knobs. Focusing on rationally designed 1DCPs composed of triarylmethyl (TAM) units, it is shown that rotation of certain aryl rings enables a transition from the trivial to the topologically non-trivial phase. Accordingly, fixing a particular twist angle configuration (e.g., via chemical functionalization) is equivalent to robustly setting a targeted topological phase. It is also found that in considered 1DCPs, the quantum phase transition occurs without the electronic band gap closing, due to a multiradical antiferromagnetic phase emerging at the transition point. All in all, this study highlights the potential of aryl ring twisting for engineering topological properties in carbon nanomaterials and establishes TAM 1DCPs as exotic topological 1D systems.

1. Introduction

Topological insulators are a class of materials characterized by an insulating band gap in their bulk and topologically protected conducting states at their surface or edges.[1,2] These appealing materials have received a huge amount of attention in the last decades,[3–6] and are currently being considered as the basis of fault-tolerant "topological" quantum computation.[7,8] Recently, it has been shown that topologically-protected states may be finely engineered in bottom-up on-surface synthesized carbon nanostructures, such as graphene nanoribbons[9–11] (GNRs) or 1D conjugated polymers (1DCPs).[12,13] A great advantage of such a bottom-up approach is the atomically precise character of the resulting carbon nanomaterials, which opens the door to tailoring topological physics at the molecular level as a means toward molecular-based quantum technologies.[14,15]

The topological character of such type of π-conjugated 1D nanostructures is frequently characterized experimentally via the detection of in-gap states pinned at the ends of the polymer chain, in analogy to the surface states in 3D topological insulators.[4–6] The presence of such boundary states is associated with the so-called topologically non-trivial phase, whereas the trivial phase corresponds to the absence of boundary states.[16] The archetypical example to understand topological physics in

I. Alcón, L. M. Canonico, J.-H. Garcia, A. W. Cummings, M. Pruneda, S. Roche
Catalan Institute of Nanoscience and Nanotechnology (ICN2)
CSIC and BIST
Campus UAB, Bellaterra, Barcelona 08193, Spain
E-mail: isaac.alcon@icn2.cat; mpruneda@cinn.es

N. Papior
Computing Center
Technical University of Denmark
Kongens Lyngby DK-2800, Denmark

The ORCID identification number(s) for the author(s) of this article can be found under https://doi.org/10.1002/adfm.202409174

DOI: 10.1002/adfm.202409174

J.-C. Tremblay
Laboratoire de Physique et Chimie Théoriques
CNRS-Université de Lorraine
UMR 7019, ICPM, Metz 57070, France

M. Pruneda
Nanomaterials and Nanotechnology Research Centre (CINN)
CSIC
Avenida de la Vega 4-6, El Entrego 33940, Spain

M. Brandbyge
Department of Physics
Technical University of Denmark
Kongens Lyngby DK-2800, Denmark

B. Paulus
Institut für Chemie und Biochemie
Physikalische und Theoretische Chemie
Freie Universität Berlin
Arnimallee 22, 14195 Berlin, Germany

S. Roche
ICREA
Institució Catalana de Recerca i Estudis Avançats
Barcelona 08070, Spain

1D is polyacetylene (PA), which is usually described with the Su–Schrieffer–Heeger (SSH) model.[17] PA is a π-conjugated linear chain of sp^2 carbon atoms with alternating double bonds (**Figure 1a**). In its primitive unit cell, composed of two C sites, two distinct electronic configurations are possible: one with the π-electrons paired within the cell and one with π-electrons paired between cells. These two configurations correspond to the topologically trivial and non-trivial phases, respectively, and while being equivalent in the periodic system, they give rise to the absence, or presence, of in-gap states pinned at the two ends of a finite PA segment, as mentioned above. In PA, the trivial phase arises when the intra-cell bond length (BL_1 in Figure 1a) is smaller than the inter-cell bond length (BL_2), $BL_1 < BL_2$, and vice versa for the non-trivial phase ($BL_1 > BL_2$). This is so because bond length is the primary structural parameter determining electronic coupling (resonance integrals) between neighboring C atoms along the PA chain. At the transition point, where $BL_1 = BL_2$, the SSH model predicts the closure of the electronic bandgap and thus a metallic state (middle panel in Figure 1a).[10] Consequently, engineering topological phases are equivalent to tunning intra-cell versus inter-cell electronic couplings, as done in PA via BL_1 and BL_2.

Such topological engineering has primarily been achieved experimentally by careful rational design of the molecular structure of carbon nanomaterials,[10,11] though alternative mechanisms have been proposed such as the application of electric fields[18] or top-down atomically-precise hydrogenation.[13] Interestingly, the intrinsic correlation between topology and π-conjugation[12,19] suggests that aryl ring twist angles could also become a powerful tool in this regard.[20] This is because aryl ring twisting determines the overlap between the p_z orbitals of the ring unit and the rest of the π-conjugated system, as studied in the past.[21–24] More recently, aryl ring twisting has been shown to enable control over electron pairing (i.e., electronic coupling) in 1DCPs and 2D conjugated polymers (2DCPs),[25,26] and it is amenable to manipulation via chemical functionalization,[24] electric fields[27] or uniaxial strain.[25] Therefore, aryl ring rotation appears to be a potential versatile knob to engineer carbon-based topological physics.[15] However, to the best of our knowledge, the relationship between aryl ring twist angles and topological character in π-conjugated nanomaterials remains to be established.

In this work, using first principles density functional theory (DFT) calculations, we demonstrate the intrinsic correlation between aryl ring twist angles and electronic topology in 1DCPs. To do so, we focus on a special type of 1DCP that may be obtained by connecting sp^2 C sites in PA via aryl rings, as depicted in Figure 1b. In the resulting structures, which are effectively 1D polymers of ring-sharing triarylmethyl (TAM) units (see below), intra-/inter-cell electronic coupling may be finely tuned via the intra-/inter-cell aryl ring dihedral angle (φ_1 and φ_2 in Figure 1b). We find that ring rotation may thus be used to transition from topologically trivial to non-trivial phases, and we propose the dihedral angle difference, $\varphi_1 - \varphi_2$, as the key parameter determining the topological class in the considered systems. Topology is characterized by computing the Zak phase for the periodic systems and by evaluating the presence/absence of in-gap states at the boundaries of finite-size 1DCPs.[9–12] Significantly, we find that in such TAM-based 1DCPs, the trivial and non-trivial phases are connected via a multiradical antiferromagnetic (AFM) transition state – that is, avoiding the metallic electronic solution (predicted by the SSH model) that manifests at higher energy. Our findings highlight the ability of aryl ring twisting to engineer the topological nature of carbon/organic nanostructures. Additionally, we demonstrate that TAM 1DCPs serve as examples of exotic topological materials displaying a quantum phase transition not involving the closure of the electronic band gap.[28]

2. Results and Discussion

Our considered 1DCPs may be thought of as 1D chains of ring-sharing TAM molecules, as depicted in Figure 1c. TAMs are the oldest class of organic radicals,[29] being composed of three aryl rings bound to a central carbon atom (αC) where their unpaired electron mainly resides (Figure 1c).[23] Because of the electronic delocalization dependence on aryl ring twist angles,[23] already exploited in TAM-based 2DCPs[25,30] and 1DCPs,[26] rotation of aryl rings should enable tuning of the αC-αC coupling (Figure 1c) and thus the topological phase of the system. If we define φ_1 and φ_2 as the intra-cell and inter-cell aryl ring twist angles, respectively, their difference, $\Delta\varphi = \varphi_1 - \varphi_2$, should be the main parameter determining the system's topology (Figure 1b). In order to evaluate this, herein we focus on the triphenylmethyl-based 1DCP (H-1DCP; Figure 1e) and two partially chlorinated derivatives (Cl-1DCP and Cl'−1DCP in Figures 1d,f respectively) where every other in-chain ring is perchlorated and thus highly twisted. Due to the high conformational flexibility of H-1DCP (low steric hindrance of H atoms) and thus its available aryl ring rotational degree of freedom, we choose this material to study how the electronic structure of 1DCPs evolves upon monotonically moving from $\Delta\varphi \ll 0$ to $\Delta\varphi \gg 0$. On the other hand, Cl- and Cl'−1DCPs are included to assess whether specific chemical designs may be used to fix a particular $\Delta\varphi$ value and, consequently, a particular topological phase.

To optimize the atomic and electronic structure of each material, we use the PBE0 hybrid functional[31] as implemented in FHI-AIMS,[32] which is an all-electron code using atom-centered numerical basis sets[33] (see Methods for details). This setup has been shown to properly capture the electronic structure of TAM nanorings[34] and 2DCPs[35] as reported in various experiments.[36,37] Due to the possible existence of multiradical magnetic phases (e.g., AFM) in TAM materials generally,[38–40] and TAM 1DCPs concretely,[26,41–43] we compare results from spin-restricted and spin-unrestricted setups throughout the manuscript. For spin-unrestricted simulations, we always set an AFM arrangement of αC spins as an initial guess, to help the simulation find possible energetically favorable broken-symmetry electronic solutions.[44]

We start by evaluating the electronic structure of H-1DCP upon varying $\Delta\varphi$ from −58 to +58 degrees. Each conformation along the $\Delta\varphi$ window is obtained by fixing the z-coordinate of carbon atoms in phenyl rings 1 and 2 (Figure 1b) while optimizing the rest of the atomic structure (see Methods for full details). At $\Delta\varphi = -58°$ the intra-cell ring is fully flat (i.e., $\varphi_1 = 0°$) whereas the inter-cell ring is twisted by 58°, and vice-versa for $\Delta\varphi = +58°$. Therefore, upon moving $\Delta\varphi$ from −58 to +58 degrees we simultaneously rotate the intracell ring out of the plane ($\varphi_1 = 0° \rightarrow 58°$) and the intercell ring into the plane ($\varphi_2 = 58° \rightarrow 0°$). At $\Delta\varphi = 0°$, phenyl rings 1 and 2 are equally twisted by 29 degrees, which

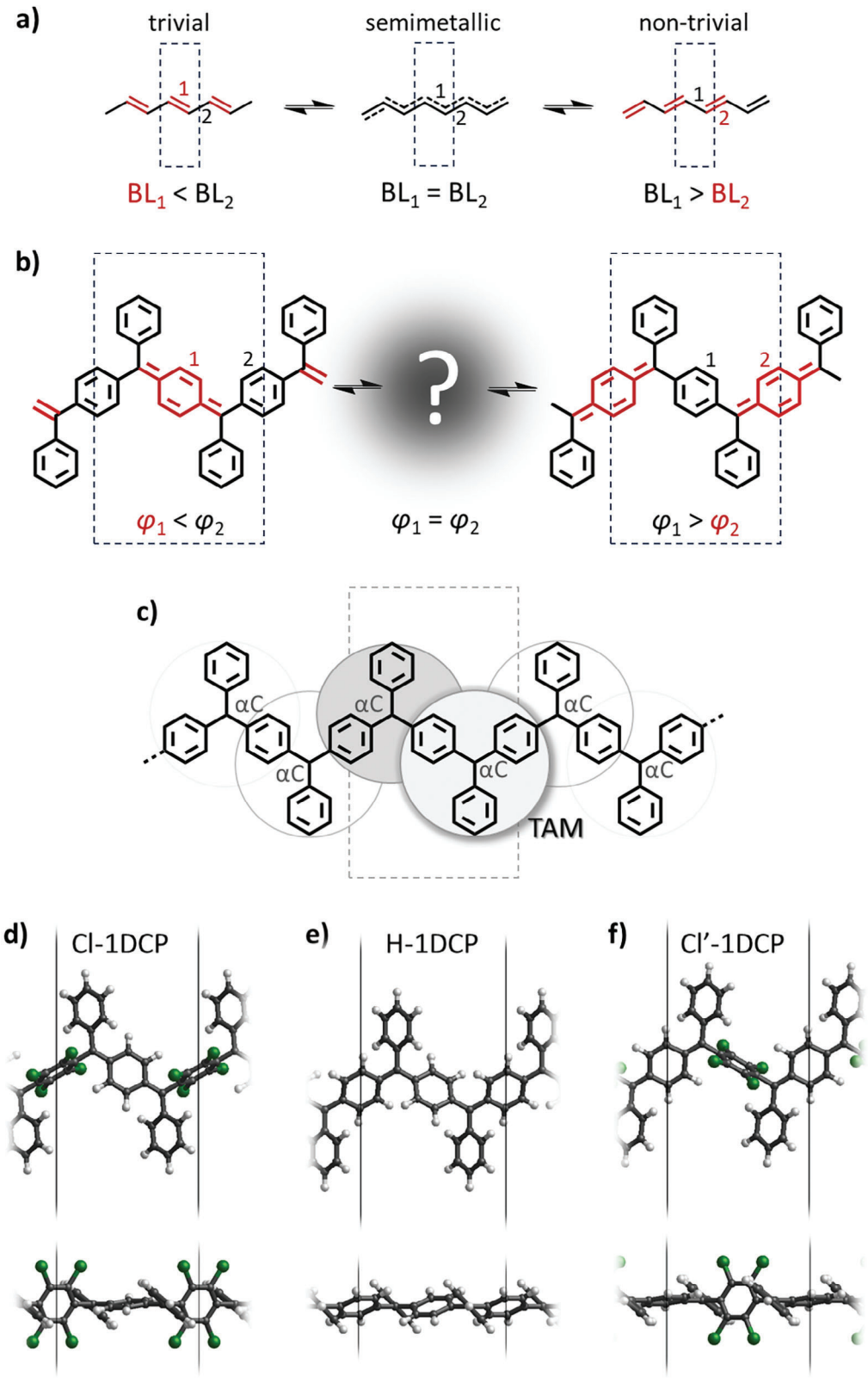

Figure 1. Schematic of the π-conjugated structure of a) PA and b) 1DCPs, highlighting local π-electron pairing in red and its correlation with bond lengths (BL) and dihedral angles (φ) for PA and 1DCPs, respectively. c) Structure of 1DCPs highlighting their composition as a 1D chain of ring-sharing TAM units. "αC" denotes the central carbon site bound to the three aryl rings in every TAM compound. Z-view (top) and y-view (bottom) of the DFT-optimized periodic structures of d) Cl-1DCP, e) H-1DCP, and f) Cl'−1DCP (see Methods for DFT optimization details).

corresponds to their mean dihedral angle in the fully optimized conformation. As seen in **Figure 2**a, the band structure of H-1DCP is essentially the same at $\Delta\varphi = -58°$ and $\Delta\varphi = +58°$, displaying a finite band gap that separates the equally dispersing valence and conduction bands. We note that this qualitative picture is independent of the level of theory utilized (e.g., restricted vs unrestricted) as shown in Figure S1 (Supporting Information). If we take a look at the spatial distribution of the valence band (VB; see Methods for details), shown in Figure 2a, we may recognize the electron-paired quinoidal configuration located either within the cell ($\Delta\varphi = -58°$) or between cells ($\Delta\varphi = +58°$), in agreement with our prior assignment in Figure 1b (red fragments). On the other hand, the perchlorated aryl rings in Cl-1DCP (Figure 1d) and Cl'−1DCPs (Figure 1f) lead to $\Delta\varphi$ values of −65 and +65 degrees, respectively, in their most stable conformation (i.e., without any structural constraints). The resulting electronic structure is qualitatively the same as for H-1DCP at $\Delta\varphi = \pm 58°$ (see Figure S2, Supporting Information) and we only note the less dispersing valence/conduction bands in the chlorated 1DCPs, in agreement with their larger $\Delta\varphi$ values inducing a higher electron localization (see red arrows in Figure S2, Supporting Information).

In order to characterize the topological class of the 1DCPs, we compute the Zak phase using the SISL code[45] for the VB associated with the electron-paired quinoidal configuration (Figure 2a). The Zak phase is given by

$$\gamma_n = i\left(\frac{2\pi}{a}\right)\int_{-\pi/a}^{\pi/a} dk \left\langle u_{nk}\middle|\frac{\partial u_{nk}}{\partial k}\right\rangle \quad (1)$$

where a is the unit cell length along the polymer direction (x in our case), n is the electronic band index, and u_{nk} is the periodic part of the corresponding Bloch state.[9] As summarized in Table S1 (Supporting Information), we find that γ_{VB} equals 0 for H-1DCP at $\Delta\varphi = -58°$ and Cl-1DCP ($\Delta\varphi = -65°$) and π for H-1DCP at $\Delta\varphi = 58°$ and Cl'−1DCP ($\Delta\varphi = 65°$). Therefore, we associate 1DCPs with $\Delta\varphi < 0$ to the trivial phase, and those with $\Delta\varphi > 0$ to the non-trivial phase (see bottom panel in Figure 2a). We note that this classification is independent of the computational setup (spin restricted vs unrestricted) as shown in Table S1 (Supporting Information). This result already confirms that φ_1 and φ_2 play the same "topological role" in 1DCPs (Figure 1b) as BL_1 and BL_2 do in PA (Figure 1a).

To better understand the transition between the two topological phases, in Figure 2 we show various key quantities as a function of $\Delta\varphi$ for H-1DCP. As seen in Figure 2b, within a spin-restricted setup (dashed curve) the transition from the trivial to the non-trivial phase passes through the closure of the electronic band gap. This result is in line with predictions based on the SSH model and prior studies using tight-binding Hamiltonians and spin-restricted DFT.[10,12] This is confirmed by the resulting metallic band structure obtained at $\Delta\varphi = 0°$ (Figure 2c). By extracting the bond-length alternation (BLA) along the $\Delta\varphi$ window (Figure S3, Supporting Information), it may be noted that the trivial to non-trivial transition involves a quinoid-to-aromatic (aromatic-to-quinoid) transformation of the intra-cell (inter-cell) ring, in full agreement with the VB wave-functions shown in Figure 2a.

As explained above, TAM 2DCPs and 1DCPs are susceptible to hosting multiradical AFM phases that could become energetically favorable along the $\Delta\varphi$ path.[25,26,34,35,40] In order to evaluate such a possibility, we calculate the quantum phase transition in a spin-unrestricted setup with an αC AFM initial guess (see Methods). To detect possible broken-symmetry solutions, we extract the average of the absolute αC spin populations, $\langle|\mu_{\alpha C}|\rangle$, at each $\Delta\varphi$ point. This quantity is proportional to the spin-polarization magnitude, and allows us to differentiate between open-shell ($\langle|\mu_{\alpha C}|\rangle > 0$) and closed-shell ($\langle|\mu_{\alpha C}|\rangle = 0$) electronic configurations.[25,35] As seen in Figure 2e, $\langle|\mu_{\alpha C}|\rangle$ emerges upon approaching $\Delta\varphi = 0°$, displaying a maximum at this point. As shown in the inset in Figure 2e, this finite $\langle|\mu_{\alpha C}|\rangle$ is associated with a multiradical electronic solution displaying antiparallel αC spins (AFM ordering). We note that such type of multiradical AFM states were previously experimentally reported for TAM 2DCPs,[37] and have been assigned to a Mott insulating phase.[40] The $\langle|\mu_{\alpha C}|\rangle$ fully disappears toward the two opposite $\Delta\varphi$ ends ($|\Delta\varphi| \gg 0°$); that is, when approaching the trivial or non-trivial topological regions. As seen in Figure 2b (solid curve), this alternative spin-unrestricted path connects the trivial and non-trivial phases without closing the electronic band gap, as confirmed in the associated band structure at $\Delta\varphi = 0°$ (Figure 2d). This finding is in line with the assignment of such AFM states to a correlated Mott insulating phase.[34,40] If we compare the relative energies of the two possible quantum transition pathways (Figure 2f), it is found that the multiradical AFM transition state (solid curve at $\Delta\varphi = 0°$) lies 0.125 eV below the metallic transition state (dashed curve at $\Delta\varphi = 0°$). To the best of our knowledge, this is the first 1D carbon nanomaterial (including GNRs and 1DCPs) displaying a topological quantum phase transition via a gapped, multiradical AFM phase. This finding is in line with prior studies demonstrating that the trivial and non-trivial phases may be connected via gapped broken-symmetry solutions.[28] Thus, instead of displaying a direct trivial to non-trivial transition (via band-gap closing), the quantum phase transition in TAM 1DCPs goes through a correlated phase where time-reversal symmetry is broken (AFM state) as a detour around the metallic transition point sitting at higher energy (see Figure 2f). We emphasize that this alternative transition route is only captured by using spin-unrestricted calculations and by setting a broken-symmetry (AFM) initial guess.[44] It is also worth noting that the π-conjugated transformation of intra- and inter-cell rings remains the same as that obtained within the spin-restricted setup (see BLA comparison in Figure S3, Supporting Information). However, the emergence of the multiradical AFM phase leads to a more progressive transition between quinoid and aromatic configurations, as opposed to the sharper change observed in the spin-restricted setup (Figure S3, Supporting Information).

The large $|\Delta\varphi|$ values for Cl-1DCP (−65°) and Cl'−1DCP (+65°) push their electronic structures deep within the trivial and non-trivial phases, respectively, and so they both remain well separated from the AFM $\Delta\varphi$ region (see empty circles in Figure 2e). The large band gaps in these chlorinated 1DCPs nicely follow the $\Delta\varphi$ trend of H-1DCP, as depicted with empty circles (spin unrestricted) and crosses (spin restricted) in Figure 2b. This suggests that the sole electronic role of aryl ring perchlorination is imposing, via steric hindrance, a high $|\Delta\varphi|$ value.

Experimentally, the topologically trivial (non-trivial) nature of this type of system is frequently inferred by detecting the presence (absence) of in-gap states pinned at the polymer's ends.[10–12]

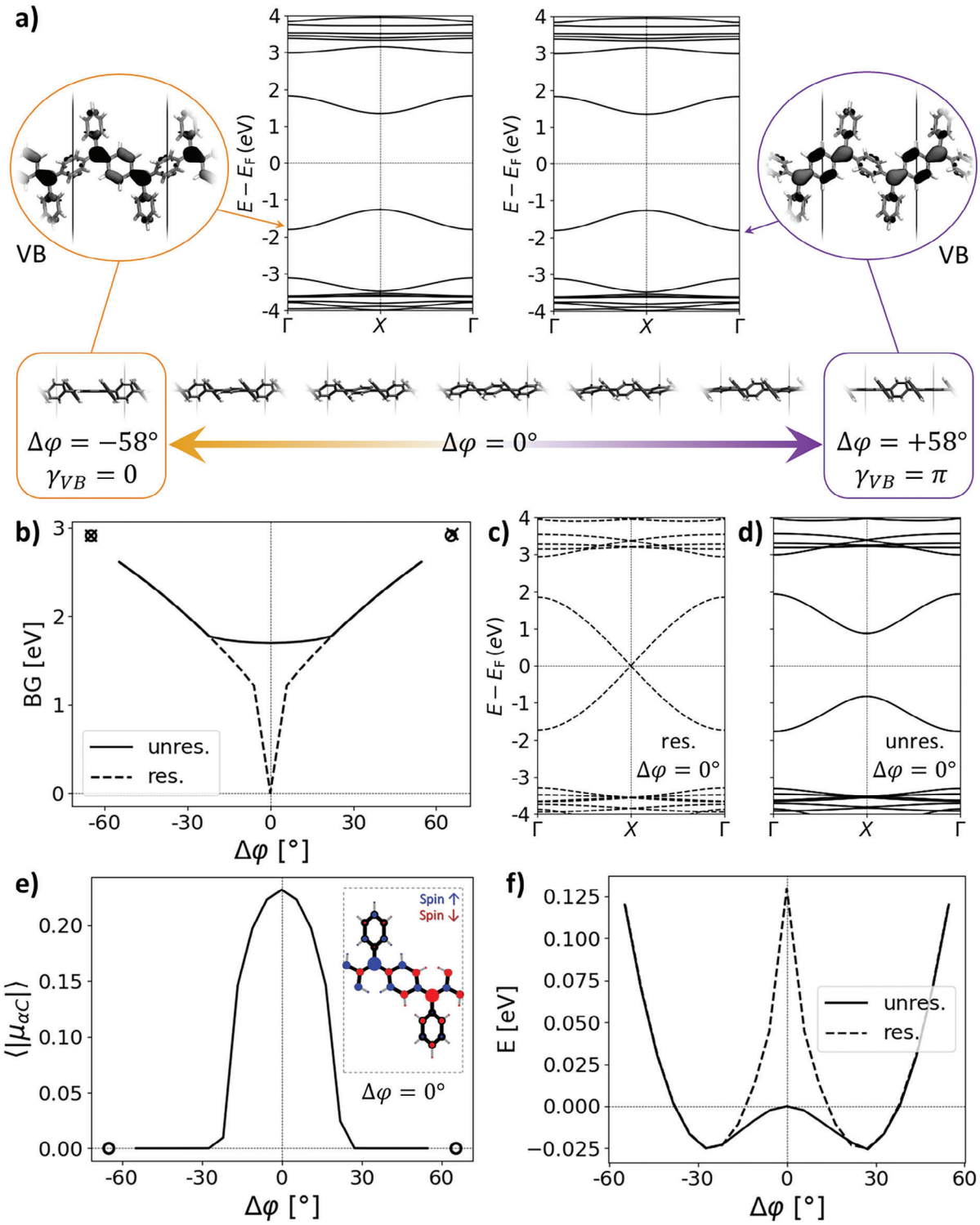

Figure 2. a) H-1DCP band structure and VB wave-function (Γ point; iso-surface value: 0.040 e bohr^{-3}) at $\Delta\varphi = -58°$ (left side) and $\Delta\varphi = +58°$ (right side), as calculated with the spin-restricted setup. The y-view of the H-1DCP structure for varying $\Delta\varphi$ is shown in the bottom panel. b) Electronic band gap of H-1DCP along the $\Delta\varphi$ window (spin-restricted: dashed curve; spin-unrestricted: solid curve). Band structures at $\Delta\varphi = 0°$ are shown for c) spin-restricted and d) unrestricted setups. e) Mean of the absolute αC spin populations ($\langle|\mu_{\alpha C}|\rangle$) and f) relative total energy against $\Delta\varphi$, the latter setting all energies with respect to the spin-unrestricted solution at $\Delta\varphi = 0°$. Dashed and solid curves correspond to the spin-restricted and unrestricted setups, the latter using an AFM initial guess on αC atoms. Cl- and Cl'−1DCPs are represented, where needed, with crosses (spin-restricted) and empty circles (spin-unrestricted). A spin-density map (spin up: blue; spin down: red) is provided as an inset in e) for $\Delta\varphi = 0°$, displaying the emergent multiradical AFM electronic solution corresponding to d).

In the following, we evaluate the $\Delta\varphi$-dependence of such boundary states in an H-1DCP fragment (i.e., an H-oligomer) built by repeating the primary unit cell ten times. We note that the two ends of the H-oligomer are passivated with hydrogen atoms to reproduce the clean molecular terminations that are typically obtained with bottom-up synthesis. As before, we compare results from spin-restricted and unrestricted setups (see Methods). **Figure** 3a shows the orbital energies of the five highest occupied molecular orbitals (HOMOs) and the five lowest unoccupied molecular orbitals (LUMOs) upon varying $\Delta\varphi$ from −58 to +58 degrees and using a spin-restricted setup. The transition from the trivial ($\Delta\varphi = -58$) to the non-trivial ($\Delta\varphi = +58$) phase is accompanied by the appearance of in-gap states pinned at the middle of the bandgap; that is, zero mode states, in full agreement with prior predictions on topological 1DCPs.[12] Figure 3b shows the HOMO wave function at $\Delta\varphi = -58°$, which displays the typical electron-paired quinoidal configuration (e.g., Figure 1b, left) and resides in the middle region of the oligomer, decaying away at each boundary. This bulk character is still maintained at $\Delta\varphi = 0°$ (Figure S4, Supporting Information). However, moving to positive $\Delta\varphi$ values leads to the appearance of mid-gap states which are localized at each end of the H-oligomer (see Figure 3c). These edge states are singly occupied molecular orbitals (SOMOs) and resemble the typical SOMO wave function of an isolated TAM mono-radical.[46] The emergence of boundary states at $\Delta\varphi = 58°$ fully agrees with our previous characterization of the H-1DCP as topologically non-trivial at such $\Delta\varphi$ values (see Zak phases in Table S1, Supporting Information). This result echoes scanning tunnelling microscopy measurements of topologically non-trivial acene 1DCPs and GNRs.[10–12]

The total energy variation of H-oligomer throughout the $\Delta\varphi$ window, as calculated with the spin-restricted setup, is shown in Figure 3d (dashed curve). Contrary to H-1DCP (Figure 2f), the total energy as a function of $\Delta\varphi$ is not symmetric around $\Delta\varphi = 0°$, with the global energy minimum sitting on the trivial side (i.e., at $\Delta\varphi < 0°$). This is so because in the trivial phase, all αC π-electrons are paired, whereas in the non-trivial phase, two αC electrons remain unpaired (i.e., the end SOMO states), which is a less energetically favorable situation (i.e., thermodynamically unstable). In the periodic systems the trivial and non-trivial phases are physically equivalent, and thus energetically degenerate (Figure 2f). However, as for the periodic system (Figure 2f), there exists an alternative path at lower energy connecting the trivial and non-trivial phases which may only be found with a spin-unrestricted setup (solid curve in Figure 3d). As for the periodic system, this path goes through a multiradical transition state and is detected through an increase in $\langle|\mu_{\alpha C}|\rangle$ (Figure 3e), which is also associated with an AFM ordering of αC spin moments (see spin-density map in Figure S5, Supporting Information). Contrary to the periodic case, $\langle|\mu_{\alpha C}|\rangle$ does not completely vanish at the non-trivial side of the $\Delta\varphi$ window (Figure 3e), owing to the spin-polarized character of boundary states in such spin-unrestricted simulations (Figure S5, Supporting Information).

This alternative topological transition pathway does not lead to states appearing right in the middle of the gap (Figure 3f) as occurring in the spin-restricted simulations (Figure 3a). However, we note that in-gap states do emerge at $\Delta\varphi = +58°$ sitting very close in energy to the bulk eigenstates (see arrow 2 at $\Delta\varphi = +58°$ in Figure 3f). Such in-gap states are indeed boundary states (Figure 3h), despite being spin-polarized as shown in the associated spin-polarized maps (Figure S5, Supporting Information). As for the spin-restricted calculations, at $\Delta\varphi = -58°$ the H-oligomer falls into the trivial phase, characterized by a null spin polarization (see Figure S5, Supporting Information) and quinoidal-like HOMOs now resolved by spin-channel (see Figure S6, Supporting Information). Contrarily, at $\Delta\varphi = 0°$ the spin-up (blue iso-contours) and spin-down (red iso-contours) channels of the HOMO wave function spatially split into the two distinct αC lattices (Figure 3g) defined by each of the two αCs in the periodic unit cell (Figure 1c). Such splitting resembles the AFM spin distribution obtained at $\Delta\varphi = 0°$ (Figure S5, Supporting Information) associated with the multiradical transition state, as in the H-1DCP (see inset in Figure 2e).

Finally, as shown for the periodic systems (Figure 2), a rational perchlorination of specific aryl rings may push the system toward the trivial (Cl-oligomer) or non-trivial (Cl'-oligomer) phases, leading to the expected bulk/edge character of the associated orbitals (Figures S7 and S8, Supporting Information). Prior studies have shown that such type of partial chlorination allows one to fix a large $\Delta\varphi$ value even under thermal fluctuations at 300 K.[26] As a result, in such chlorinated-1DCPs, the multiradical AFM phase is completely avoided even under the effect of bond vibrations at room temperature. This is in contrast to the H-1DCP, which undergoes a dynamic equilibrium between open-shell (AFM) and closed-shell configurations under the same conditions.[26] This suggests that perchlorination of aryl rings is a promising tool to realize highly robust end states in 1DCPs.

3. Conclusion

In summary, we have demonstrated that TAM 1DCPs may host trivial and non-trivial topological states, which may be finely tailored via control of aryl ring twist angles. The key parameter determining the topological class is the dihedral angle difference between the two in-chain aryl rings present in the primary unit cell, $\Delta\varphi$. It is found that $\Delta\varphi < 0°$ leads to the topological trivial phase, whereas $\Delta\varphi > 0°$ leads to the non-trivial phase, which is confirmed both by the Zak characterization of the valence band in the periodic systems and by the existence/absence of boundary states in the corresponding oligomers. As previously found in other types of 1DCPs,[12] topology is intrinsically linked with π-conjugation and, consequently, we observe quinoid-to-aromatic (and aromatic-to-quinoid) transformations along the topological phase transition (see BLA analysis in Figure S3, Supporting Information). Significantly, while spin-restricted simulations predict a metallic transition state at $\Delta\varphi = 0°$, in line with prior studies and the SSH model, an alternative AFM multiradical transition state that sits lower in energy is found via spin-unrestricted simulations. Such a multiradical phase, previously associated with a correlated Mott-insulating phase for TAM 2DCPs,[34,40] displays a finite band gap. To the best of our knowledge, this is the first case of a 1D carbon nanomaterial evidencing a topological quantum phase transition via a correlated AFM Mott insulating phase. It is worth noting that such multiradical states tend to be thermodynamically unstable (i.e., chemically reactive) and are sensitive to charge-transfer effects,[47] making it very challenging to detect them on metallic surfaces.[48,49] Finally, it is also shown that the rational chemical

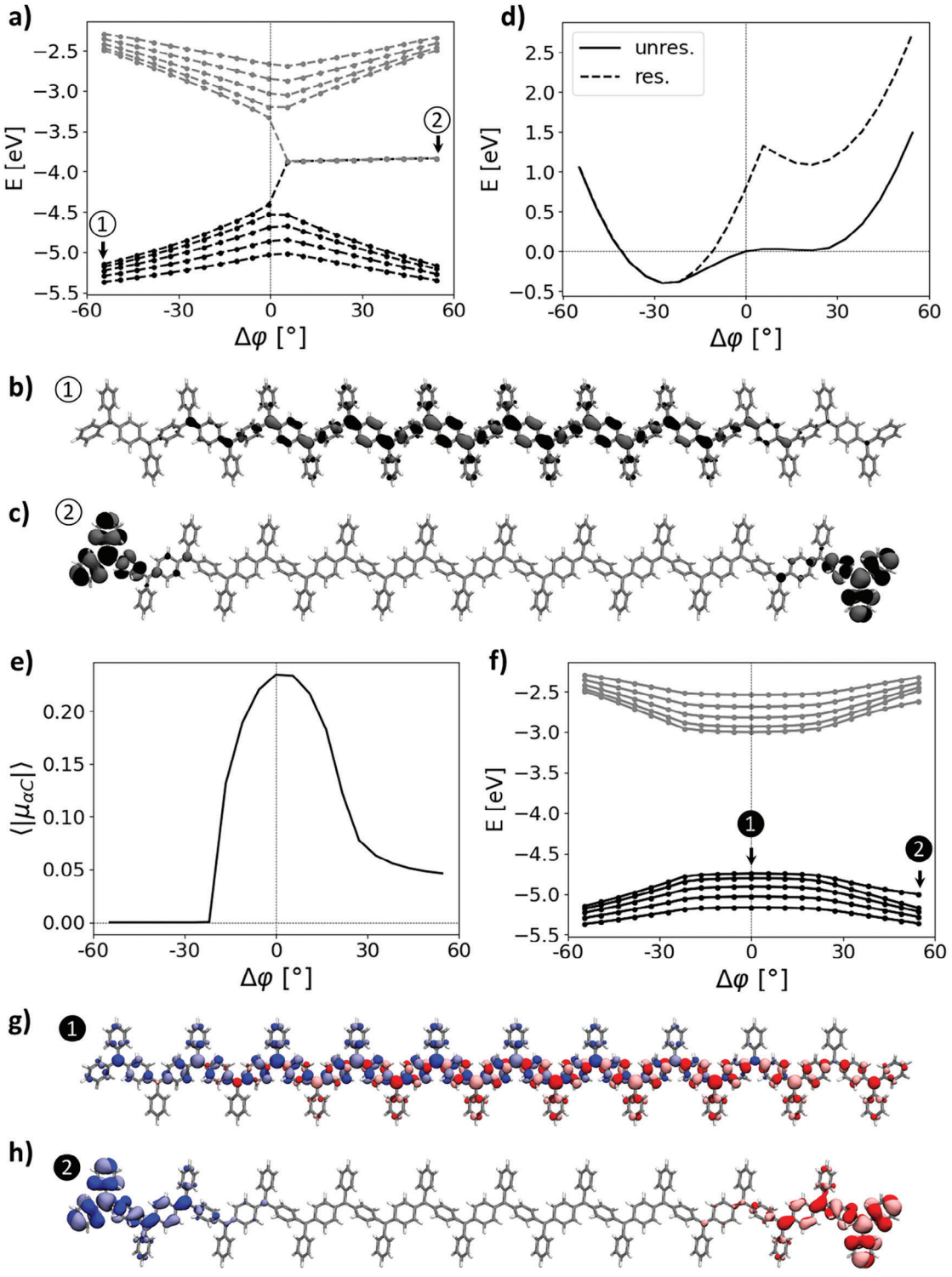

Figure 3. a) H-oligomer orbital energies of the five top HOMOs (black dots) and five bottom LUMOs (grey dots) upon varying $\Delta\varphi$ from −58 to +58 degrees, as calculated in a spin-restricted setup. b) Spatial distribution of the top HOMO wave function at $\Delta\varphi = -58°$ and c) SOMO wave function at $\Delta\varphi = +58°$, obtained with spin-restricted calculations. d) Relative total energy of H-oligomer throughout the $\Delta\varphi$ window as calculated with a spin-restricted setup (dashed curve) and an unrestricted setup (solid curve), the latter using an αC spin-polarized AFM initial guess. e) $\langle|\mu_{\alpha C}|\rangle$ versus $\Delta\varphi$ for the spin-unrestricted setup and f) associated orbital energies for the same set of HOMOs and LUMOs depicted in (a). g) Spatial distribution of the HOMO wave function at $\Delta\varphi = 0°$ and h) the SOMO wave functions at $\Delta\varphi = +58°$, resolved by spin-channel (spin-up: blue; spin-down: red). Darker (lighter) colors represent the positive (negative) phase of the wave function (iso-surface value: 0.015 e Bohr $^{-3}$). Spatially plotted wave functions are indicated with labeled arrows (1, 2) in (a) and (f).

design of the 1DCP allows, via steric hindrance effects, to push the system toward $\Delta\varphi \ll 0°$ (Cl-1DCP) or $\Delta\varphi \gg 0°$ (Cl'−1DCP) which, in turn, fixes the resulting electronic ground state within the topologically trivial or non-trivial phase, respectively.

Overall, our work adds aryl ring twist angles to the structural/chemical toolkit to engineer topological states in π-conjugated nanostructured materials, which could ultimately open the door to controlling topological phases via external manipulation of ring rotation using mechanical strain,[25,30,50] compression,[34] or perpendicular electric fields,[27] among others.[51] Our study also highlights the importance of searching for spin-polarized broken symmetry solutions along the quantum phase transition, as their existence (completely missed in a spin-restricted setup) has strong implications both for the resulting electronic properties (e.g., band gap) and the system's thermodynamic stability (with important implications for, e.g., chemical reactivity).[52,53] Finally, we have also established a connection between the fields of TAMs and topological physics, and we hope that future studies will benefit from our findings to unveil novel topological effects in other similar TAM-based materials, such as the highly studied TAM 2DCPs.[34,37,39,40]

4. Experimental Section

The main results of this study have been obtained with DFT simulations using the PBE0 hybrid functional[31] and a Tier-1 light numerical atom-centered orbital (NAO) basis set,[54] as implemented in the FHI-AIMS code.[32] Periodic simulations have used a 36 k-points Γ-centred Monkhorst-pack k-mesh. Constrained optimizations were carried out to assess the dependence of the electronic structure of H-1DCP on $\Delta\varphi$. Since the H-1DCP plane was set parallel to the x-y plane (at z = 25 Å), $\Delta\varphi$ was fixed by freezing the z-coordinate of αC atoms (two per unit cell) and all carbon atoms within in-chain aryl rings (i.e., intra-cell ring and inter-cell ring, as shown in red in Figure 1b) while optimizing all other atomic coordinates. Due to the periodicity of H-1DCP along *x*, the corresponding cell vector was also optimized at each $\Delta\varphi$ point. The $\Delta\varphi$ window was scanned by starting from the most symmetrical structure, where $\Delta\varphi = 0°$ ($\varphi_1 = \varphi_2 = 29°$) and twisting toward $\Delta\varphi < 0°$ ($\varphi_1 < \varphi_2$) and $\Delta\varphi > 0°$ ($\varphi_1 > \varphi_2$), separately. Such twisting was done by rotating out-of-plane one of the in-chain rings (i.e., increasing φ_1 or φ_2), while simultaneously rotating in-plane the other (i.e., decreasing φ_2 or φ_1). The input geometry at each $\Delta\varphi$ point was obtained via aryl ring rotation on the structure optimized in the previous $\Delta\varphi$ step, thus ensuring a smooth transition between the different electronic phases. Structural optimizations converged once the total energy change between consecutive steps was below $1{\cdot}10^{-5}$ eV and the maximum force component (per atom) was below 10 meV Å^{-1}. The $\Delta\varphi$ window was separately calculated for spin-restricted DFT and spin-unrestricted DFT, the latter using an αC antiparallel spin configuration (AFM) as the electronic initial guess at each $\Delta\varphi$ step. This computational setup was also used to optimize the periodic structure of Cl-1DCP and Cl'−1DCP, though in such cases aryl ring twist angles were not constrained during energy minimization. From these calculations, most of the target quantities were extracted, such as electronic band structures, band gaps, spin-populations (e.g., $\langle|\mu_{\alpha C}|\rangle$) and total energies.

For the computation of the Zak-phase, calculated for the extreme $\Delta\varphi$ values, single-point calculations were done on top of the PBE0-optimized 1DCP structures using the PBE functional[55] as implemented in the SIESTA code.[56] It was noted that such PBE simulations (SIESTA) provide qualitatively the same electronic structure as obtained with PBE0 (FHI-AIMS), as shown in Figures S1 and S2 (Supporting Information). There one may see a renormalization of the band gap as the most significant difference between the two computational setups. The SISL utility[45] was used to extract the Zak phase associated with the valence band obtained from such PBE calculations (see Table S1, Supporting Information).

Oligomers are constructed from the 1DCP structure by repeating ten times the unit cell and properly terminating the two ends of the oligomer, thus reproducing the atomically precise molecular ends typically obtained via bottom-up synthesis. Such construction procedure is done for every $\Delta\varphi$ point and DFT setup (i.e., spin-restricted and unrestricted). The same constraints, level of theory (PBE0, FHI-AIMS), and convergence criteria are used to optimize the atomic structure of the resulting H-oligomer. As for periodic calculations, Cl-oligomer and Cl'oligomer are optimized without fixing aryl ring twist angles. Spin-restricted and unrestricted calculations are set up as explained above.

Supporting Information

Supporting Information is available from the Wiley Online Library or from the author.

Acknowledgements

I.A. is grateful for a Juan de la Cierva postdoctoral grant (FJC2019-038971-I) from the Ministerio de Ciencia e Innovación (MCIN). L.M.C. also acknowledges a Juan de la Cierva postdoctoral grant (FJC2021-047300-I) from MCIN. M.P. acknowledges support from PID2022-139776NB-C61, funded by MCIN/AEI/10.13039/501100011033/FEDER, U. E. A. C. and S. R. acknowledge support from PID2019-106684GB-I00 also funded by MCIN/AEI/10.13039/501100011033/FEDER, UE. Computer facilities of the Freie Universität Berlin (ZEDAT) are acknowledged for computer time. We acknowledge support of the publication fee by the CSIC Open Access Publication Support Initiative through its Unit of Information Resources for Research (URICI). ICN2 is funded by the CERCA Programme from Generalitat de Catalunya, has been supported by the Severo Ochoa Centres of Excellence programme [SEV-2017-0706], and is currently supported by the Severo Ochoa Centres of Excellence programme, Grant CEX2021-001214-S, both funded by MCIN/AEI/10.13039.501100011033.

Conflict of Interest

The authors declare no conflict of interest.

Data Availability Statement

The data that support the findings of this study are available from the corresponding author upon reasonable request.

Keywords

antiferromagnetism, aryl ring twist, boundary-states, conjugated polymers, density functional theory, quantum-phase transition, topological-phases

Received: May 28, 2024
Revised: July 16, 2024
Published online: July 30, 2024

[1] M. Z. Hasan, C. L. Kane, *Rev. Mod. Phys.* **2010**, *82*, 3045.
[2] J. E. Moore, *The Birth of Topological Insulators*, *Vol. 464*, Nature Publishing Group, Berlin, **2010**, pp. 194–198.

[3] C. L. Kane, E. J. Mele, *Phys. Rev. Lett.* **2005**, *95*, 146802.
[4] L. Fu, C. L. Kane, E. J. Mele, *Phys. Rev. Lett.* **2007**, *98*, 106803.
[5] M. Z. Hasan, J. E. Moore, *Annu. Rev. Condens. Matter Phys.* **2011**, *2*, 55.
[6] X. L. Qi, S. C. Zhang, *Rev. Mod. Phys.* **2011**, *83*, 1057.
[7] C. Nayak, S. H. Simon, A. Stern, M. Freedman, S. Das Sarma, *Rev. Mod. Phys.* **2008**, *80*, 1083.
[8] S. D. Sarma, M. Freedman, C. Nayak, *npj Quantum Inf* **2015**, *1*, 15001.
[9] T. Cao, F. Zhao, S. G. Louie, *Phys. Rev. Lett.* **2017**, *119*, 076401.
[10] O. Gröning, S. Wang, X. Yao, C. A. Pignedoli, G. Borin Barin, C. Daniels, A. Cupo, V. Meunier, X. Feng, A. Narita, K. Müllen, P. Ruffieux, R. Fasel, *Nature* **2018**, *560*, 209.
[11] D. J. Rizzo, G. Veber, T. Cao, C. Bronner, T. Chen, F. Zhao, H. Rodriguez, S. G. Louie, M. F. Crommie, F. R. Fischer, *Nature* **2018**, *560*, 204.
[12] B. Cirera, A. Sánchez-Grande, B. de la Torre, J. Santos, S. Edalatmanesh, E. Rodríguez-Sánchez, K. Lauwaet, B. Mallada, R. Zbořil, R. Miranda, O. Gröning, P. Jelínek, N. Martín, D. Ecija, *Nat. Nanotechnol.* **2020**, *15*, 437.
[13] H. González-Herrero, J. I. Mendieta-Moreno, S. Edalatmanesh, J. Santos, N. Martín, D. Écija, B. Torre, P. Jelinek, *Adv. Mater.* **2021**, *33*, 2104495.
[14] F. Lombardi, A. Lodi, J. Ma, J. Liu, M. Slota, A. Narita, W. K. Myers, K. Müllen, X. Feng, L. Bogani, *Science* **2019**, *366*, 1107.
[15] H. Wang, H. S. Wang, C. Ma, L. Chen, C. Jiang, C. Chen, X. Xie, A. P. Li, X. Wang, *Nat. Rev. Phys.* **2021**, *3*, 791.
[16] J. Li, S. Sanz, N. Merino-Díez, M. Vilas-Varela, A. Garcia-Lekue, M. Corso, D. G. de Oteyza, T. Frederiksen, D. Peña, J. I. Pascual, *Nat. Commun.* **2021**, *12*, 5538.
[17] W. P. Su, J. R. Schrieffer, A. J. Heeger, *Phys. Rev. Lett.* **1979**, *42*, 1698.
[18] F. Zhao, T. Cao, S. G. Louie, *Phys. Rev. Lett.* **2021**, *127*, 166401.
[19] M. Corso, D. G. de Oteyza, *Nature Research* **2020**, *15*, 421.
[20] B. Yuan, C. Li, Y. Zhao, O. Gröning, X. Zhou, P. Zhang, D. Guan, D. Guan, Y. Li, Y. Li, H. Zheng, H. Zheng, C. Liu, C. Liu, Y. Mai, P. Liu, W. Ji, J. Jia, J. Jia, S. Wang, S. Wang, *J. Am. Chem. Soc.* **2020**, *142*, 10034.
[21] M. J. S. Dewar, *J. Am. Chem. Soc.* **1952**, *74*, 3345.
[22] F. C. Adam, S. I. Weissman, *J. Am. Chem. Soc.* **1958**, *80*, 2057.
[23] I. Alcón, S. T. Bromley, *RSC Adv.* **2015**, *5*, 98593.
[24] L. Venkataraman, J. E. Klare, C. Nuckolls, M. S. Hybertsen, M. L. Steigerwald, *Nature* **2006**, *442*, 904.
[25] I. Alcón, R. Santiago, J. Ribas-Arino, M. Deumal, I. de P. R. Moreira, S. T. Bromley, *Nat. Commun.* **2021**, *12*, 1705.
[26] I. Alcón, J. Shao, J. C. Tremblay, B. Paulus, *RSC Adv.* **2021**, *11*, 20498.
[27] K. Jutglar Lozano, R. Santiago, J. Ribas-Arino, S. T. Bromley, *Phys. Chem. Chem. Phys.* **2021**, *23*, 3844.
[28] M. Ezawa, Y. Tanaka, N. Nagaosa, *Sci. Rep.* **2013**, *3*, 2790.
[29] M. Gomberg, *J. Am. Chem. Soc.* **1900**, *22*, 757.
[30] I. Alcón, D. Reta, I. de P. R. Moreira, S. T. Bromley, *Chem. Sci.* **2017**, *8*, 1027.
[31] C. Adamo, V. Barone, *J. Chem. Phys.* **1999**, *110*, 6158.
[32] V. Blum, R. Gehrke, F. Hanke, P. Havu, V. Havu, X. Ren, K. Reuter, M. Scheffler, *Comp. Phys. Comm.* **2009**, *180*, 2175.
[33] V. Havu, V. Blum, P. Havu, M. Scheffler, *J. Comput. Phys.* **2009**, *228*, 8367.
[34] R. Santiago, I. Alcón, J. Ribas-Arino, M. Deumal, I. P. R. Moreira, S. T. Bromley, *Adv. Funct. Mater.* **2020**, *31*, 2004584.
[35] I. Alcón, F. Viñes, I. de P. R. Moreira, S. T. Bromley, *Nat. Commun.* **2017**, *8*, 1957.
[36] Z. Li, T. Y. Gopalakrishna, Y. Han, Y. Gu, L. Yuan, W. Zeng, D. Casanova, J. Wu, *J. Am. Chem. Soc.* **2019**, *141*, 16266.
[37] J. Wu, S. Wu, M. Li, H. Phan, D. Wang, T. S. Herng, J. Ding, Z. Lu, *Angew. Chem., Int. Ed.* **2018**, *57*, 8007.
[38] N. M. Shishlov, *Russ. Chem. Rev.* **2006**, *75*, 863.
[39] Y. Yang, C. Liu, X. Xu, Z. Meng, W. Tong, Z. Ma, C. Zhou, Y. Sun, Z. Sheng, *Polym. Chem.* **2018**, *9*, 5499.
[40] S. Thomas, H. Li, J.-L. Bredas, *Adv. Mater.* **2019**, *31*, 1900355.
[41] D. R. Mañeru, I. de P. R. Moreira, F. Illas, *J. Am. Chem. Soc.* **2016**, *138*, 5271.
[42] J. Shao, I. Alcón, B. Paulus, J. C. Tremblay, *J. Phys. Chem. C* **2021**, *125*, 25624.
[43] D. Braun, P. Lehmann, *Die Makromol. Chemie* **1976**, *177*, 1387.
[44] A. Zunger, *Nat. Comput. Sci.*, **2022**, *2*, 529.
[45] N. Papior, *sisl* **2021**, p. https://github.com/zerothi/sisl.
[46] X. Ai, E. W. Evans, S. Dong, A. J. Gillett, H. Guo, Y. Chen, T. J. H. Hele, R. H. Friend, F. Li, *Nature* **2018**, *563*, 536.
[47] I. Alcón, G. Calogero, N. Papior, A. Antidormi, K. Song, A. W. Cummings, M. Brandbyge, S. Roche, *J. Am. Chem. Soc.* **2022**, *144*, 8278.
[48] T. Wang, A. Berdonces-Layunta, N. Friedrich, M. Vilas-Varela, J. P. Calupitan, J. I. Pascual, D. Peña, D. Casanova, M. Corso, D. G. de Oteyza, *J. Am. Chem. Soc.* **2022**, *144*, 4522.
[49] E. C. H. Wen, P. H. Jacobse, J. Jiang, Z. Wang, S. G. Louie, M. F. Crommie, F. R. Fischer, *J. Am. Chem. Soc.* **2023**, *145*, 19338.
[50] I. Alcón, S. T. Bromley, *Phys. Chem. Chem. Phys.* **2018**, *20*, 5028.
[51] C. Moreno, X. Diaz de Cerio, M. Vilas-Varela, M. Tenorio, A. Sarasola, M. Brandbyge, D. Peña, A. Garcia-Lekue, A. Mugarza, *J. Am. Chem. Soc.* **2023**, *145*, 8988.
[52] I. Ratera, J. Veciana, *Chem. Soc. Rev.* **2012**, *41*, 303.
[53] I. Ratera, J. Vidal-Gancedo, D. Maspoch, S. T. Bromley, N. Crivillers, M. Mas-Torrent, *Perspectives for Polychlorinated Trityl Radicals*, Vol. *9*, Royal Society of Chemistry, London, **2021**, pp. 10610–10623.
[54] I. Y. Zhang, X. Ren, P. Rinke, V. Blum, M. Scheffler, *New J. Phys.* **2013**, *15*, 123033.
[55] J. P. Perdew, K. Burke, M. Ernzerhof, *Phys. Rev. Lett.* **1996**, *77*, 3865.
[56] J. M. Soler, E. Artacho, J. D. Gale, A. García, J. Junquera, P. Ordejón, D. Sánchez-Portal, *J. Phys. Condens. Matter* **2002**, *14*, 2745.